Hindawi
Concepts in Magnetic Resonance Part A
Volume 2019, Article ID 5040465, 7 pages
https://doi.org/10.1155/2019/5040465

Research Article

Dual-Echo Arterial Spin Labeling for Brain Perfusion Quantification and Functional Analysis

André Monteiro Paschoal,[1] **Fernando Fernandes Paiva**,[2] **and Renata Ferranti Leoni**[1]

[1] *Departamento de Física, FFCLRP, Universidade de São Paulo, Ribeirão Preto, SP, Brazil*
[2] *Instituto de Física de São Carlos, Universidade de São Paulo, São Carlos, SP, Brazil*

Correspondence should be addressed to Renata Ferranti Leoni; leonirf@usp.br

Received 28 March 2019; Accepted 19 June 2019; Published 1 August 2019

Academic Editor: Claudio Luchinat

Arterial Spin Labeling (ASL) is a noninvasive MRI-based method to measure cerebral blood flow (CBF). Recently, the study of ASL as a functional tool has emerged once CBF fluctuation comes from capillaries in brain tissue, giving a more spatially specific response when compared to the standard functional MRI method, based on the blood oxygenation level-dependent (BOLD) contrast. Although the BOLD effect could be desirable to study brain function, if one aims to quantify CBF, such effect is considered contamination that can be more attenuated if short TE value is used in the image acquisition. An approach that provides both CBF and function information in a simultaneous acquisition is the use of a dual-echo ASL (DE-ASL) readout. Our purpose was to evaluate the information provided by DE-ASL regarding CBF quantification and functional connectivity with a motor task. Pseudocontinuous ASL of twenty healthy subjects (age: 32.4 ± 10.2 years, 13 male) was acquired at a 3T scanner. We analyzed the influence of TE on CBF values and brain connectivity provided by CBF and concurrent BOLD (cc-BOLD) time series. Brain networks were obtained by the general linear model and independent component analysis. Connectivity matrices were generated using a bivariate correlation (Fisher Z values). No effect of the sequence readout, but significant effect of the TE value, was observed on gray matter CBF values. Motor networks with reduced extension and more connections with important regions for brain integration were observed for CBF data acquired with short TE, proving its higher spatial specificity. Therefore, it was possible to use a dual-echo readout provided by a standard commercial ASL pulse sequence to obtain reliable quantitative CBF values and functional information simultaneously.

1. Introduction

Arterial Spin Labeling (ASL) is a magnetic resonance (MR) perfusion-weighted technique with the advantage of not using an exogenous contrast agent. It is achieved by using the arterial blood as an endogenous tracer, which is magnetically labeled (label image) through the application of radiofrequency (RF) pulses. Such pulses are applied in a strategic position (labeling plane) so that the magnetization in the region of interest (ROI) is changed compared to a non-label situation (control image) [1, 2]. With this set of images, cerebral blood flow (CBF) is estimated from the subtraction between control and label images. Due to the ASL intrinsic low signal-to-noise ratio (SNR), there is the necessity of acquiring multiple control-label pairs, and the CBF map is the mean of all subtractions executed [3]. On the other hand, the temporal series of ASL images allows the evaluation of CBF fluctuations over time, from which functional information can be estimated [4–6].

Although in functional magnetic resonance imaging (fMRI) the blood oxygen level-dependent (BOLD) contrast is mainly used, applications of ASL in functional studies have increased over the last years mainly because of two reasons. First, while BOLD contrast depends on a complex combination of blood oxygenation, cerebral blood volume (CBV), CBF, and metabolic rate of oxygen (CMRO2), ASL provides quantitative information of one physiologic parameter (CBF) [7, 8]. Second, ASL has a better spatial specificity to neuronal

activity when compared to BOLD [9–13]. Moreover, ASL combined with dual-echo readout (DE-ASL) is an interesting approach to optimize the acquisition aimed at both CBF quantification and functional analysis [14]. Images acquired using short echo time (TE) are more weighted in perfusion, while the use of longer TE increases the effect of transversal relaxation ($T2^*$), typical of the BOLD contrast [6, 15].

Some previous reports used DE-ASL to evaluate the correlation between CBF time series and the concomitant BOLD (cc-BOLD) signal, either in resting state or with a visual/motor task condition, and analyze the functional connectivity [16–21]. Lu and colleagues showed the influence of BOLD contamination on the temporal dynamics of ASL curve but did not analyze its effects on functional connectivity [17]. Regarding acquisition and analysis, Ghariq and colleagues investigated some specific aspects of the signal and suggested the use of background suppression to reduce BOLD contamination and to increase CBF sensibility [16]. Moreover, Storti and colleagues recently reported the contribution of ASL to understand how CBF is related to functional connectivity [19] and the feasibility of DE-ASL to analyze brain function [20]. However, they did not evaluate the method regarding the direct effect of TE in CBF quantification, cc-BOLD and CBF networks, and functional analysis.

Therefore, we aimed to evaluate the CBF quantification with DE-ASL in comparison with standard ASL acquisition, analyze the similarity of networks between CBF and cc-BOLD and between each TE used, and verify changes in brain connectivity for different TE values.

2. Methods

2.1. Subjects. Twenty healthy participants (age: 32.4 ± 10.2 years, 13 male) were scanned on a 3T Achieva MRI Scanner (Philips Healthcare, Best, Netherlands) equipped with a 32-channel receive head coil. All subjects gave their written informed consent after the ethics committee of the institution approved the study.

2.2. Image Acquisition and Protocol. DE-ASL data were acquired using a 2D echo-planar imaging (EPI) readout and a pseudo-continuous labeling (pCASL) scheme with the following parameters: TR = 4000 ms, TE_1/TE_2 = 9/28 ms, labeling duration/postlabeling delay = 1450/1550 ms, 20 slices, slice thickness = 5 mm, spatial resolution = 3.75 x 3.75 mm^2, FOV = 240 x 240 mm^2, flip angle = 90°, and total acquisition time of 4.26 min. For conventional single-echo pCASL, the same parameters were used for both TE values (9 and 28 ms). No background suppression was used. In addition, a structural 3D gradient-echo T1-weighted scan was performed with TR = 7 ms, TE = 3.2 ms, FOV = 240 x 240 mm^2, 180 slices, slice thickness = 1 mm, spatial resolution = 1 x 1 mm^2, flip angle = 8°.

The experimental protocol was a block design paradigm alternating rest and right-hand finger tapping. Each block had duration of 32 seconds (8 volumes), totalizing four blocks of rest and four blocks of motor task. The command to the subject to start or stop the task was shown in a monitor: red screen during rest blocks and green screen for the task blocks.

2.3. Image Processing. Imaging preprocessing was performed using local scripts in MATLAB (MathWorks, Natick, MA) in combination with Statistical Parametric Mapping (SPM12, http://www.fil.ion.ucl.ac.uk/spm/software/spm12/). Structural T1-weighted images were used for segmentation and obtaining the gray matter (GM) and white matter (WM) masks. For ASL images, we adapted scripts from ASLtbx [22] performing the following steps: motion correction, coregistration to anatomical image and masks, temporal filtering, and spatial smoothing through the application of an isotropic Gaussian kernel (FWHM = 4 mm for CBF quantification and FWHM = 6 mm for functional images).

2.4. CBF Quantification. Perfusion maps were generated by the subtraction of control and label images. For basal CBF analysis, we used the sync subtraction, while for functional analysis we performed a running pairwise subtraction to increase the number of perfusion images [23]. Quantification was based on the General Kinetic Model [8] using the following parameters: blood longitudinal relaxation time ($T1_b$) = 1650 ms; labeling efficiency = 0.85; blood/tissue water partition coefficient (GM/WM) = 0.98/0.84 g/mL; tissue T1 (GM/WM) = 1020/770 ms calculated using a Look-Locker sequence [24]. Finally, CBF time series and mean CBF map were normalized to MNI standard space (resolution = 2 x 2 x 2 mm^3; matrix size: 79 x 95 x 79).

2.5. General Linear Model. We ran a general linear model (GLM) analysis using FSL (http://fsl.fmrib.ox.ac.uk/fsl/fslwiki) to assess the differences regarding CBF and cc-BOLD networks between TE values. Both CBF and cc-BOLD information were obtained using FEAT to preprocess and perform the statistical analysis according to the following steps: subject motion correction (MCFLIRT [25]), brain extraction, spatial smoothing filtering (FWHM = 5 mm), temporal filtering, coregistration to MNI atlas, whitening, GLM analysis according to experimental design, and finally the clustering analysis. The obtained networks were spatially compared by the Dice Similarity Coefficient (DSC) [26] using local scripts in MATLAB.

2.6. Independent Component Analysis Networks. The functional analysis was performed using CONN Toolbox [27], in which CBF time series were detrended and filtered with a low-pass filter ($f < 0.07$). To remove the signal from white matter and cerebrospinal fluid we used principal component analysis (PCA) with the CompCor algorithm. Then, we ran the independent component analysis (ICA) algorithm setting 20 individual components previously.

Next, we selected the motor network that resulted from ICA from CBF maps obtained with each echo to evaluate the difference between them regarding spatial similarity and functional connectivity. For spatial similarity,

Table 1: Main anatomical regions activated during the finger-tapping task and the corresponding number of activated voxels.

TE_1	Number of voxels	TE_2	Number of voxels
Left Precentral Gyrus	418	Left Precentral Gyrus	431
Left Postcentral Gyrus	407	Left Postcentral Gyrus	500
Right Precentral Gyrus	384	Right Precentral Gyrus	489
Left Superior Parietal Lobule	292	Left Superior Parietal Lobule	281
Right Postcentral Gyrus	265	Right Postcentral Gyrus	176
Right Superior Parietal Lobule	169	Right Superior Parietal Lobule	241

we used the DSC calculated in MATLAB. We also analyzed the difference between groups in Z scores and performed a one-sample t-test using the R Project [28] to obtain a p-value matrix considering only significant differences ($p < 0.05$, corrected for multiple comparisons using Bonferroni-Holm method). Finally we evaluated the differences in functional connectivity between the two CBF time series.

3. Results

3.1. CBF Comparison between Single- and Dual-Echo pCASL. We compared the mean CBF values for gray matter acquired with different sequences and TEs to evaluate how such parameters affected the CBF quantification. Figure 1 shows CBF maps obtained with standard single-echo and dual-echo readouts. No significant difference in gray matter CBF values was observed for different readouts but the same TE. Mean values for TE_1 were 35.50 ± 11.23 mL/100g/min and 36.08 ± 9.45 mL/100 g/min, respectively, for single- and dual-echo acquisitions ($p = 0.95$). For TE_2 mean values were 21.84 ± 8.15 mL/100 g/min and 22.16 ± 6.74 mL/100 g/min, respectively, for single- and dual-echo acquisitions ($p = 0.95$). However, significant differences were observed when comparing CBF for different TE values but the same readout ($p < 0.05$), due to the T2 decay present in images acquired with longer TE value.

Considering only the motor cortex, for TE_1, CBF values were 41.58 ± 12.61 mL/100 g/min and 36.46 ± 14.21 mL/100g/min, respectively, for single- and dual-echo acquisitions ($p = 0.48$). And for TE_2, CBF values were 28.28 ± 8.22 mL/100g/min and 27.38 ± 9.69 mL/100g/min, respectively, for single- and dual-echo acquisitions ($p = 0.88$).

3.2. GLM Analysis. Figure 2 shows the motor network of normalized CBF and cc-BOLD. We only assessed the results obtained with the DE-ASL since they were acquired during the same scan, and no variability resulted due to differences in task performance. The spatial similarity between them was higher for TE_1 (DSC = 0.4, Figure 2(a)) than for TE_2 (Figure 2(b), DSC = 0.25). Moreover, when comparing CBF (Figure 2(c)) or cc-BOLD (Figure 2(d)) network for both TE values, we observed a higher number of activated voxels for longer TE due to the higher BOLD contamination in the signal. It increases the sensitivity of the method to detect brain activation but decreases its spatial specificity. Such contamination can be seen on CBF time series for the longer TE. Figure 3 shows the mean CBF time series for all voxels of the motor network activated by the finger-tapping task normalized to the mean CBF of first rest condition block, considering all subjects.

3.3. ICA Networks. For both TE values, in a dual-echo acquisition, ICA was able to identify the following networks: motor, auditory, default mode network (DMN), visual and executive control network (ECN). A comparison of the motor network obtained for each TE showed a spatial similarity of 30% (DSC = 0.30). Table 1 shows how that difference in similarity is distributed over the anatomical regions by the different number of activated voxels in the primary motor cortex.

Figure 4 shows the connectivity patterns for the motor network obtained with both TE values of the dual-echo readout. Although for TE_2 (Figure 4(b)) the connectivity within the motor network was stronger than for TE_1 (Figure 4(a)), some connections with other brain regions, such as the precuneus, were not identified for the longer TE. Moreover, the correlation between right precentral and postcentral gyri was statistically significant ($p < 0.05$, FDR corrected) when comparing data of both TE values.

4. Discussion

The acquisition of DE-pCASL is an interesting strategy to acquire quantitative CBF and functional network information simultaneously. To guarantee that CBF is measured with the same precision as in standard pCASL scheme, we compared the results of CBF quantification for both readout schemes, EPI single- and dual-echo. We found that there is no significant difference between the gray matter CBF values obtained for each scheme. The difference in CBF between TE_1 and TE_2 was also nearly the same for single- and dual-echo schemes, in which the CBF values for TE_2 were approximately 60% of the ones for TE_1, due to T2 decay. One could account for such decay, but the lower image SNR for longer TE would

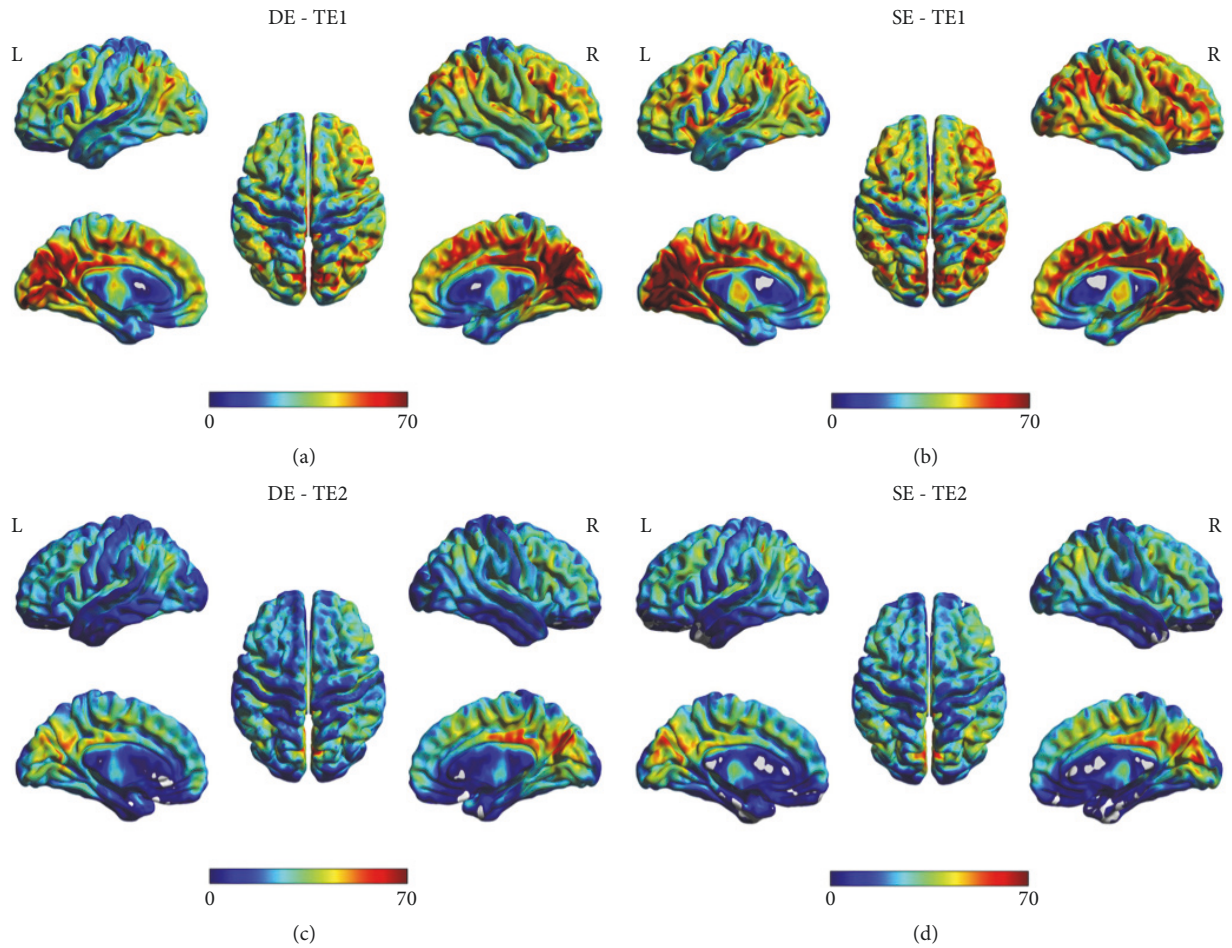

Figure 1: CBF maps obtained with different readouts (DE: dual-echo, SE: single-echo) and TE values: (a) DE, TE_1 = 10 ms; (b) SE, TE_1 = 10 ms; (c) DE, TE_2 = 28 ms; (d) SE, TE_2 = 28 ms. Color bar shows CBF range in mL/100 g/min.

still be present [29], resulting in a decrease of precision in CBF quantification. Short TE values are preferred for that case. To our knowledge, it is the first study that confirms that it is trustful to quantify CBF with DE-pCASL and short TE.

Although there was considerable spatial overlap between CBF and cc-BOLD activation maps, the similarity coefficient was not high. More activation voxels were observed for cc-BOLD, confirming its higher sensitivity but lower spatial specificity when compared to CBF signal [30, 31]. It is especially observed for the longer TE acquisition where the BOLD contamination was higher (Figure 2). Such contamination may explain the signal variability observed on CBF time series for longer TE (Figure 3). For TE_1, CBF values followed the experimental design for the finger-tapping task, in which all the four blocks were present. That behavior is not visible for TE_2 due to the lower SNR of the images, so that the effect of outliers had a high impact in the time-series profile.

Those differences in CBF signal for different TE values also reflected changes in functional connectivity. There was a significant loss of connections among primary motor cortex areas and other regions not primarily associated with motor activation, but important for brain integration, such as the precuneus. Looking specifically to the primary motor cortex, we also found significant differences in the connectivity pattern for the connection between the post- and precentral gyri, two primary anatomical areas related to motor functions.

However, our study has some limitations. First, the number of volumes acquired in each block of the acquisition paradigm was small, which may increase the effects of outliers in the temporal series, especially for the longer TE (Figure 3). However, increasing the number of volumes per block would increase significantly the total acquisition time, so that it must be considered to design the experiment. Second, our sample size may be considered small. However, we performed robust data analysis which is constantly performed in studies with similar sample size.

In conclusion, our study explored a set of information provided by the acquisition of DE-pCASL. Regarding CBF

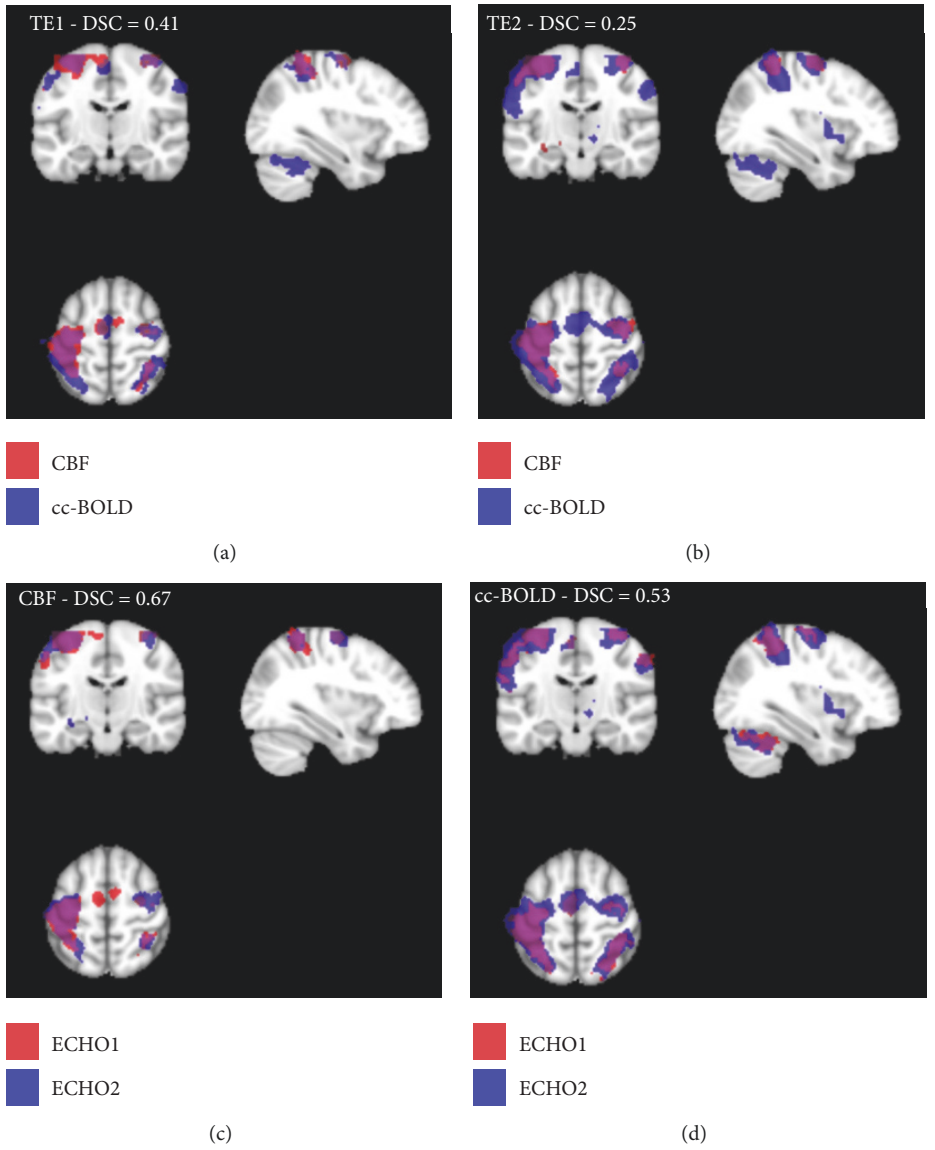

Figure 2: Comparisons of GLM results for the motor networks obtained with dual-echo readout: (a) CBF versus cc-BOLD for TE_1; (b) CBF versus cc-BOLD for TE_2; (c) TE_1 versus TE_2 for CBF networks; and (d) TE_1 versus TE_2 for cc-BOLD networks. DSC: Dice Similarity Coefficient.

quantification, we found that CBF values obtained through DE-pCASL are statistically the same as those obtained with the standard pCASL scheme. Also, for functional analysis, images acquired with short TE were successful in identifying brain networks. Our findings suggest that DE-pCASL results are trustful for both CBF quantification and functional analysis and may be a good alternative to separate acquisitions of ASL and BOLD-fMRI, reducing acquisition time without losing any of that information.

Data Availability

The magnetic resonance images used to support the findings of this study are restricted by the ethics board of the institution in order to protect the participants' privacy. Data are available from the corresponding author upon request for researchers who meet the criteria for access to confidential data.

Conflicts of Interest

The authors declare that they have no conflicts of interest.

Acknowledgments

This study was supported by CNPq (Conselho Nacional de Desenvolvimento Científico e Tecnológico).

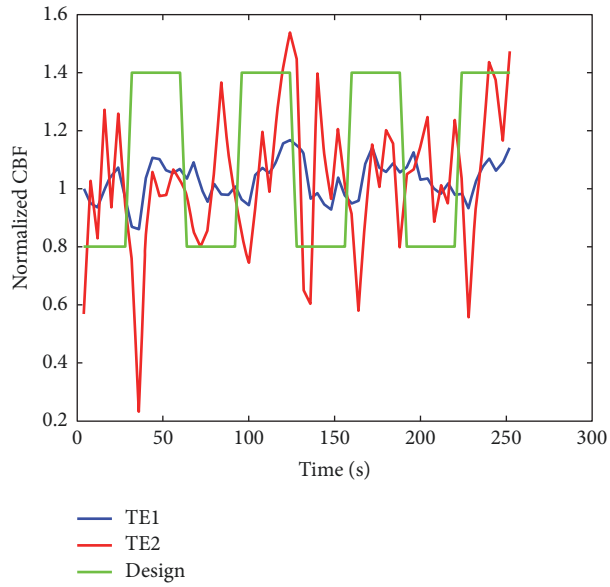

FIGURE 3: CBF time series normalized to the mean CBF of the first rest condition block for TE_1 (blue) and TE_2 (red). The experimental block design is shown in green.

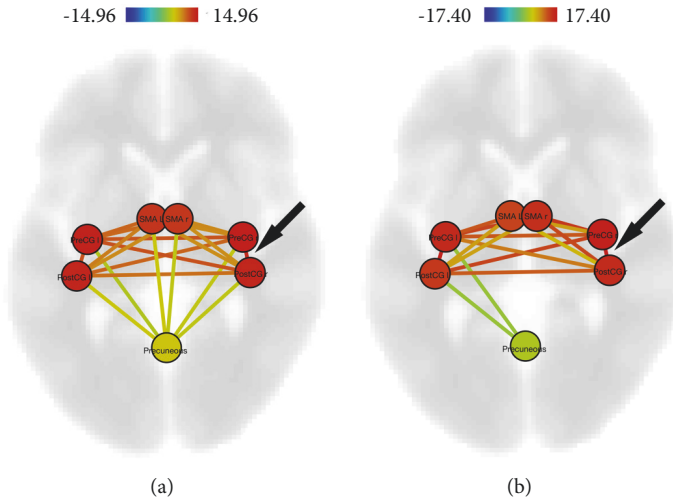

(a) (b)

FIGURE 4: Functional connectivity within the motor network for (a) TE_1 and (b) TE_2. The arrow points to the correlation that shows a significant difference when comparing TE_1 and TE_2 data. PreCG-l: left precentral gyrus; PreCG-r: right precentral gyrus; PostCG-l: left postcentral gyrus; PostCG-r: right postcentral gyrus; SMA-l: left supplementary motor area, SMA-r: right supplementary motor area, precuneus. Color bar refers to the range of T scores.

References

[1] J. A. Detre, J. S. Leigh, D. S. Williams, and A. P. Koretsky, "Perfusion imaging," *Magnetic Resonance in Medicine*, vol. 23, no. 1, pp. 37–45, 1992.

[2] J. C. Ferre, E. Bannier, H. Raoult, G. Mineur, B. Carsin-Nicol, and J. Y. Gauvrit, "Arterial spin labeling (ASL) Perfusion: techniques and clinical use," *Journal de Radiologie Diagnostique et Interventionnelle*, vol. 94, no. 12, pp. 1208–1221, 2013.

[3] E. C. Wong, R. B. Buxton, and L. R. Frank, "Quantitative perfusion imaging using arterial spin labeling," *Neuroimaging Clinics of North America*, vol. 9, no. 2, pp. 333–342, 1999.

[4] S. L. Talagala and D. C. Noll, "Functional MRI using steady-state arterial water labeling," *Magnetic Resonance in Medicine*, vol. 39, no. 2, pp. 179–183, 1998.

[5] G. K. Aguirre, J. A. Detre, E. Zarahn, and D. C. Alsop, "Experimental design and the relative sensitivity of BOLD and perfusion fMRI," *Neuroimage*, vol. 15, no. 3, pp. 488–500, 2002.

[6] E. C. Wong, R. B. Buxton, and L. R. Frank, "Implementation of quantitative perfusion imaging techniques for functional brain mapping using pulsed arterial spin labeling," *NMR in Biomedicine*, vol. 10, no. 4-5, pp. 237–249, 1997.

[7] R. B. Buxton, "Quantifying CBF with arterial spin labeling," *Journal of Magnetic Resonance Imaging*, vol. 22, no. 6, pp. 723–726, 2005.

[8] R. B. Buxton, L. R. Frank, E. C. Wong, B. Siewert, S. Warach, and R. R. Edelman, "A general kinetic model for quantitative perfusion imaging with arterial spin labeling," *Magnetic Resonance in Medicine*, vol. 40, no. 3, pp. 383–396, 1998.

[9] J. A. Detre and J. Wang, "Technical aspects and utility of fMRI using BOLD and ASL," *Clinical Neurophysiology*, vol. 113, no. 5, pp. 621–634, 2002.

[10] I. Boscolo Galazzo, S. F. Storti, E. Formaggio et al., "Investigation of brain hemodynamic changes induced by active and passive movements: a combined arterial spin labeling-BOLD fMRI study," *Journal of Magnetic Resonance Imaging*, vol. 40, no. 4, pp. 937–948, 2014.

[11] I. B. Galazzo, S. F. Storti, A. Del Felice et al., "Patient-specific detection of cerebral blood flow alterations as assessed by arterial spin labeling in drug-resistant epileptic patients," *PLoS ONE*, vol. 10, no. 5, 2015.

[12] W.-M. Luh, E. C. Wong, P. A. Bandettini, B. D. Ward, and J. S. Hyde, "Comparison of simultaneously measured perfusion and BOLD signal increases during brain activation with T-1-based tissue identification," *Magnetic Resonance in Medicine*, vol. 44, no. 1, pp. 137–143, 2000.

[13] M. A. F. Pimentel, P. Vilela, I. Sousa, and P. Figueiredo, "Localization of the hand motor area by arterial spin labeling and blood oxygen level-dependent functional magnetic resonance imaging," *Human Brain Mapping*, vol. 34, no. 1, pp. 96–108, 2013.

[14] S. Tak, D. J. Wang, J. R. Polimeni, L. Yan, and J. J. Chen, "Dynamic and static contributions of the cerebrovasculature to the resting-state BOLD signal," *NeuroImage*, vol. 84, pp. 672–680, 2014.

[15] M. W. Woolrich, P. Chiarelli, D. Gallichan, J. Perthen, and T. T. Liu, "Bayesian inference of hemodynamic changes in functional arterial spin labeling data," *Magnetic Resonance in Medicine*, vol. 56, no. 4, pp. 891–906, 2006.

[16] E. Ghariq, M. A. Chappell, S. Schmid, W. M. Teeuwisse, and M. J. van Osch, "Effects of background suppression on the sensitivity of dual-echo arterial spin labeling MRI for BOLD and CBF signal changes," *NeuroImage*, vol. 103, pp. 316–322, 2014.

[17] H. Lu, M. J. Donahue, and P. C. van Zijl, "Detrimental effects of BOLD signal in arterial spin labeling fMRI at high field strength," *Magnetic Resonance in Medicine*, vol. 56, no. 3, pp. 546–552, 2006.

[18] S. F. Storti, I. B. Galazzo, F. B. Pizzini, and G. Menegaz, "Dual-echo ASL based assessment of motor networks: a feasibility study," *Journal of Neural Engineering*, 2017.

[19] S. F. Storti, I. Boscolo Galazzo, S. Montemezzi, G. Menegaz, and F. B. Pizzini, "Dual-echo ASL contributes to decrypting the link between functional connectivity and cerebral blow flow," *Human Brain Mapping*, vol. 38, no. 12, pp. 5831–5844, 2017.

[20] S. F. Storti, I. B. Galazzo, F. B. Pizzini, and G. Menegaz, "Dual-echo ASL based assessment of motor networks: a feasibility study," *Journal of Neural Engineering*, vol. 15, no. 2, article 026018, 2018.

[21] A. D. Cohen, A. S. Nencka, and Y. Wang, "Multiband multi-echo simultaneous ASL/BOLD for task-induced functional MRI," *PLoS ONE*, vol. 13, no. 2, article e0190427, 2018.

[22] Z. Wang, G. K. Aguirre, H. Rao et al., "Empirical optimization of ASL data analysis using an ASL data processing toolbox: ASLtbx," *Magnetic Resonance Imaging*, vol. 26, no. 2, pp. 261–269, 2008.

[23] J. P. S. Silva, L. D. M. Mônaco, A. M. Paschoal, I. A. F. Oliveira, and R. F. Leoni, "Effects of global signal regression and subtraction methods on resting-state functional connectivity using arterial spin labeling data," *Magnetic Resonance Imaging*, vol. 51, pp. 151–157, 2018.

[24] Í. A. Oliveira, T. M. Guimarães, R. M. Souza et al., "Brain functional and perfusional alterations in schizophrenia: an arterial spin labeling study," *Psychiatry Research: Neuroimaging*, vol. 272, pp. 71–78, 2018.

[25] M. Jenkinson, P. Bannister, M. Brady, and S. Smith, "Improved optimization for the robust and accurate linear registration and motion correction of brain images," *NeuroImage*, vol. 17, no. 2, pp. 825–841, 2002.

[26] K. Jann, D. G. Gee, E. Kilroy et al., "Functional connectivity in BOLD and CBF data: similarity and reliability of resting brain networks," *NeuroImage*, vol. 106, pp. 111–122, 2015.

[27] S. Whitfield-Gabrieli and A. Nieto-Castanon, "Conn: a functional connectivity toolbox for correlated and anticorrelated brain networks," *Brain Connectivity*, vol. 2, no. 3, pp. 125–141, 2012.

[28] R Development Core T, *Computational Many-Particle Physics*, 2008.

[29] J. H. Liu and A. Venot, "Design of a computerized system for the retrospective analysis by the physician of his own drug prescriptions," *Studies in Health Technology and Informatics*, vol. 84, no. Pt 2, pp. 1175–1179, 2001.

[30] M. N. Yongbi, F. Fera, V. S. Mattay, J. A. Frank, and J. H. Duyn, "Simultaneous BOLD/perfusion measurement using dual-echo FAIR and UNFAIR: sequence comparison at 1.5T and 3.0T," *Magnetic Resonance Imaging*, vol. 19, no. 9, pp. 1159–1165, 2001.

[31] T. T. Liu and E. C. Wong, "A signal processing model for arterial spin labeling functional MRI," *NeuroImage*, vol. 24, no. 1, pp. 207–215, 2005.